Efficient heat transfer in high-power fiber lasers

Yuanyuan Fan (范元媛)[1,2,3], Bing He (何 兵)[1,2*], Jun Zhou (周 军)[1,2], Jituo Zheng (郑寄托)[1,2,3], Shoujun Dai (代守军)[1,2,3], Chun Zhao (赵 纯)[1,2], Yunrong Wei (魏运荣)[1,2], and Qihong Lou (楼祺洪)[1,2]**

[1]*Shanghai Institute of Optics and Fine Mechanics, Chinese Academy of Sciences, Shanghai 201800, China*

[2]*Shanghai Key Laboratory of All Solid-State Laser and Applied Techniques, Shanghai 201800, China*

[3]*Graduate University of Chinese Academy of Sciences, Beijing 100049, China*

[*]*Corresponding author: bryanho@siom.ac.cn;* [**]*corresponding author: junzhousd@siom.ac.cn*

Received March 10, 2012; accepted May 17, 2012; posted online August 3, 2012

The maximum output power of fiber lasers limited by the thermal degradation of double-clad fiber coatings is theoretically simulated. We investigated the thermal effects on high-power continuous wave (CW) fiber lasers with a focus on heating at the splice joints as well as on the doped fiber caused by quantum defects. Whether thermal interface materials are used or not, the thermal contact resistances between the fiber and its heat sink are measured separately while using different cooling equipments. Though the thermal management of splices is more difficult than that of active fibers, a temperature increase of 0.019 K/W is obtained for a splice joint into which the pump light launches. The splice joint sustains 3 kW of total passing power.

OCIS codes: 140.3510, 140.6810, 140.3615, 060.2320.

doi: 10.3788/COL201210.111401.

High-power, rare-earth-doped, double-clad fiber lasers have recently attracted attention in various scientific and industrial applications due to their high efficiency, compactness, reliability, and outstanding beam quality[1,2]. Given that many applications require high-power output, there is a strong demand for multi-kilowatt (kW)-level, high-brightness fiber lasers. The major problems of bulk solid-state lasers, such as stress fractures and beam distortions, can be alleviated by the long and thin geometries of fiber lasers[3]. However, thermal management is still one of the most critical issues in scaling higher output power from ytterbium-doped, double-clad fiber (YDCF) sources. Although the intrinsic large surface-to-active-volume ratio of fibers has direct and indirect advantages to heat dissipation, the use of shorter fibers with higher thermal loading densities in kW fiber lasers requires careful thermal management[4−7]. Polymer coatings needed for fiber handling have low thermal stability and are the primary limiting factors for heat load in the fiber[8]. Therefore, the thermal management of polymer coatings greatly influences the maximum output power and reliability.

Although previous works have proposed the use of thermal contact resistance to analyze the thermal effects of kW-level fiber lasers[8,9], they do not use thermal interface materials (TIMs). Given that TIMs are used to minimize the thermal contact resistance between two rigid surfaces[10], the significant power increase in fiber lasers raises a need for improved TIMs that allows efficient heat transfer across the fiber-heat sink interface, thus reducing thermal contact resistance. To minimize splice heating, which is critical for the reliability of fiber laser systems, we separately analyze the thermal contact resistances between the fiber and heat sinks when different kinds of cooling equipment are used. From these, we determine the most effective cooling method. The effectiveness of various cooling methods is experimentally determined. A splice is achieved, which has a surface temperature increase of 0.019 K/W, and is capable of sustaining 3 kW of total passing power.

The low-index polymer coatings of conventional double-clad fibers, which guide the pump light and protect the fiber, are very sensitive to high thermal loads. Therefore, low-index polymer coatings cause thermal damage when the temperatures approach the range from 150 to 200 °C (long-term reliability may require operation below 80 °C)[7]. The heat deposition density in the core has an upper limit that can be tolerated before the onset of coating damage. The following is theoretical maximum output power P_{Lmax} for a single-end pumped laser before the coating damage is reached when the quantum defect heating is assumed to provide the sole contribution to heating[11]:

$$P_{\mathrm{Lmax}} \approx \frac{4\pi(T_{\mathrm{d}}-T_{\mathrm{s}})[\frac{2}{k_{\mathrm{oc}}}\ln(\frac{r_{\mathrm{oc}}}{r_{\mathrm{ic}}})+\frac{2}{r_{\mathrm{oc}}h}]^{-1}\eta_{\mathrm{abs}}}{\alpha_p} \cdot \Big(\frac{\eta_{\mathrm{q}}v_{\mathrm{L}}}{v_{\mathrm{p}}-\eta_{\mathrm{q}}v_{\mathrm{L}}}\Big), \quad (1)$$

where T_{d} is the maximum temperature that the coating can tolerate, T_{s} is the ambient temperature (or the temperature of the heat sink), k_{oc} is the thermal conductivity of the outer cladding, r_{ic} is the radius of the inner cladding, r_{oc} is the radius of the outer cladding, h is the heat transfer coefficient, v_{L} is the lasing frequency, v_{p} is the pump frequency, α_{p} is the absorption coefficient for pump light launched into the inner cladding, η_{abs} is the fraction of pump light absorbed in the fiber, and η_{q} is the pumping quantum efficiency.

Figure 1 shows the theoretical maximum output power P_{Lmax} as a function of the heat transfer coefficient h for YDCFs with $r_{\mathrm{ic}} = 200$ μm, $r_{\mathrm{oc}} = 250$ μm, $\alpha_{\mathrm{p}} = 1.26$ dB/m, $K_{\mathrm{oc}} = 0.24$ W/mK, and $\eta_{\mathrm{abs}} \approx 1$. P_{Lmax} depends significantly on h and on the cooling (heat-sinking) conditions. For the thermal damage-free operation of cladding-pumped YDCFs at the kW power level, the heat transfer coefficient h must exceed 1 000 W/(m^2·K). Given that free convection is an order of magnitude less

efficient than conduction for dissipating heat from an optical fiber[12], heat sinks are used to cool the fiber, whereas thermal contact resistances are used to describe the heat diffusion between the fiber and heat sink.

Thermal interface resistance measures how well heat is transferred across the interface of two rigid surfaces, such as fiber and a heat sink baseplate. Air acts as a thermal barrier that prevents efficient heat transfer across the interface, because it has a very low thermal conductivity ($k_{\rm air}$ = 0.026 W/mK at room temperature). Increasing the contact pressure reduces thermal contact resistance. Meanwhile, pressure enhances the contact area between the fiber and heat sink, and reduces the amount of air remaining at the interface. Therefore, pressure reduces contact resistances, as shown in Fig. 2(a). The total thermal contact resistance of Fig. 2(a) consists of the following parallel resistances: 1) conduction resistance $R_{\rm cond}$ at the points in which the surfaces contact, and 2) conduction and radiative resistance $R_{\rm air}$ across the gaps of non-contact areas. $R_{\rm air}$ is extremely high[10]. Filling the gaps between the fiber and the heat sink with TIMs with high thermal conductivity is an advanced method that improves machining surface roughness and flatness as well as reduces thermal contact resistance (Fig. 2(b)).

The thermal contact resistance per unit surface $R''_{\rm tc}$ ($\rm m^2{\cdot}K/W$) between the fiber and the heat sink can be expressed as[7]

$$R''_{\rm tc} = \frac{T_{\rm s} - T_\infty}{q''}, \tag{2}$$

where $T_{\rm s}$ (K) is the fiber surface temperature, T_∞ (K) is the heat sink temperature, and q'' ($\rm W/m^2$) is the heat flux. For an active fiber, the heat generation q_0 ($\rm W/m^3$), the heat load q' (W/m), and the pump absorption α (dB/m) are related as

$$q_0 = (1 - 10^{-\alpha\cdot {\rm d}L/10})\frac{P\left(1 - \frac{\lambda_{\rm P}}{\lambda_{\rm s}}\right)}{\pi a^2} = \frac{q'{\rm d}L}{\pi a^2}, \tag{3}$$

where P is the pump power through a section of length dL, and $\lambda_{\rm s}$ and $\lambda_{\rm P}$ are the signal and pump wavelengths, respectively. Moreover, q'' is defined by $q'' = \frac{q'}{\rm perimeter}$.

For a point on the fiber, Fig. 3 shows the diagram of the fiber being placed in three heat sinks with different groove geometries. All the fibers dropped in the groove without any external pressure. The grooves cannot perfectly match the fibers for a given length due to the limited machining precision and the fact that the surface roughness and flatness are affected. Therefore, the interstitial air may be significant thickness in some places. For a recoated active fiber-to-fiber splice, $R''_{\rm tc}$ (shown in Fig. 3) is estimated using Eq. (2). To obtain an approximation of $R''_{\rm tc}$, assumptions were made in accordance with Ref. [7]. First, the heat transfer from fiber to air was assumed to be small enough for air to be a thermal insulator. Second, the measured temperature of the surface exposed to air was assumed to be close to the actual temperature of the fiber, which was uniform in the radial direction. Third, $R''_{\rm tc}$ was assumed to be invariant with temperature. Finally, the temperature of the heat sink T_∞ was assumed to be uniform and, without any heat load, equal to $T_{\rm s}$. From the assumptions, the heat load q' was obtained from Eq. (3). To obtain the heat flux q'', the heat load q' was divided by the perimeter, i.e., the length of the junction between the heat sink and the fiber in which heat transfer occurred. For convenience, the perimeter was calculated from the groove geometry. Some measurements used TIMs with thermal conductivities that were much higher than that of air. Temperature measurements were also separately tested for experiments, in which TIMs were or were not used. The results of the experiments and numerical calculations are shown in Table 1, where the temperature elevations are obtained through experiments.

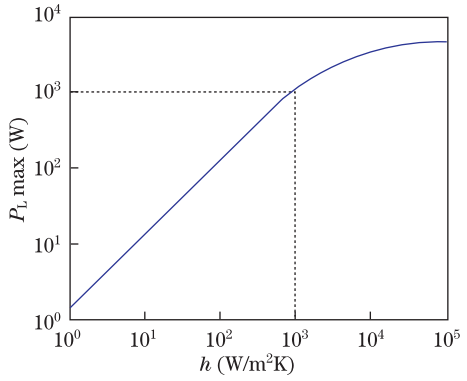

Fig. 1. Maximum output power $P_{\rm Lmax}$ (before the onset of coating damage) as a function of h.

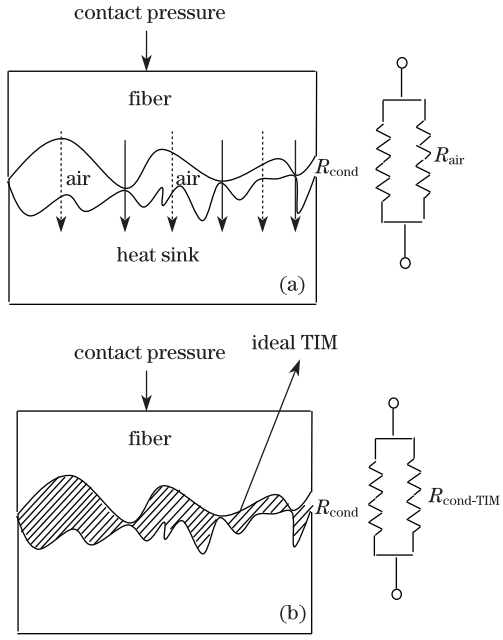

Fig. 2. Exploded view of the thermal contact resistances (a) without a TIM and (b) with an ideal TIM.

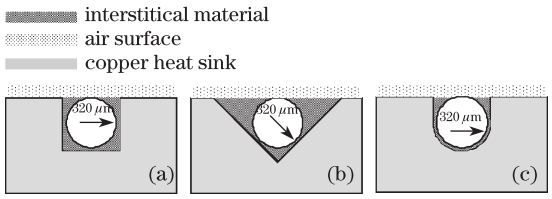

Fig. 3. Schematic representation of the setup to determine $R''_{\rm tc}$.

Table 1. Thermal Contact Resistances for All Three Groove Geometries

Recoated Fiber Splice Parameter (μm)	80/400/600		
Geometry	Fig. 3(a)	Fig. 3(b)	Fig. 3(c)
Perimeter of the Geometry (μm)	1 860	2 128	1 605
Recoated Fiber Splice External Radius (μm)	600	600	600
Pump Absorption at 976 nm (dB/m)	8	8	8
Quantum Efficiency	0.90	0.90	0.90
Pump Power at Test Position (W)	150	150	150
Heat Load at Test Power (W/m)	12.6	12.6	12.6
Temperature Elevation of Fiber with a TIM (K)	25	41	22
Temperature Elevation of Fiber with a TIM (K)	10.5	17.2	10.9
$R''_{tc} \times 10^{-3}$ without a TIM (m^2·K/W)	3.69	6.92	2.8
$R''_{tc} \times 10^{-3}$ with a TIM (m^2·K/W)	1.55	2.9	1.39

For a given groove geometry, the thermal contact resistance with a TIM is much smaller than that without a TIM; hence, better cooling is achieved with a TIM. For a given TIM, the thermal contact resistance varies depending on the groove geometry. In this letter, assumptions were made to obtain an approximation of R''_{tc}. Therefore, the uncertainty is high. Although R''_{tc} has been roughly determined, its order of magnitude shows that thermal contact resistance significantly contributes to the heating of fibers. R''_{tc} varies greatly depending on the designs. Therefore, the results in Table 1 cannot be used to accurately determine the temperature increase of the fiber for cooling equipment with different values of R''_{tc}.

Many factors limit the reduction of R''_{tc} in actual operations; these include the pressure on the fiber, the surface roughness of the heat sink, the matching between the recoated spliced fiber and the grooves, and the like. Therefore, a more precise matching between the grooves and the fiber is preferred. Figure 4 shows the microscope image of the grooves used in the experiment. The images show that the surface roughness of the heat sink can still be improved.

A backward-pumped, all-fiber laser configuration was built in order to test the cooling capabilities of a gain fiber with a TIM (Fig. 3(c)). Figure 5 shows the experimental setup. All the components were connected by recoated fusion splices, which made the system more compact and reliable. The laser oscillator consisted of a pair of fiber Bragg gratings (FBGs), YDCF, and a $(6+1)\times 1$ combiner. A 20-m YDCF section (Nufern Inc.) was used as the gain medium. The absorption coefficient of the YDCF section was 1.26 dB/m at 976 nm. The fiber had a core with a 20-μm diameter and an octagonal-shaped inner cladding with a diameter of 400 μm. The laser cavity consisted of a pair of FBGs; one was used as the high reflector (FBG1, $R > 99\%$ for LP_{01} mode at 1 079 nm) and the other as the output

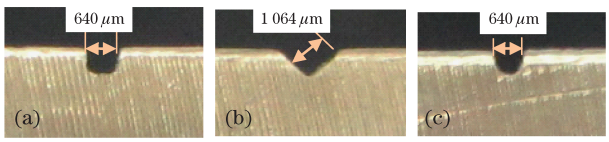

Fig. 4. Microscopic images of the three kinds of grooves.

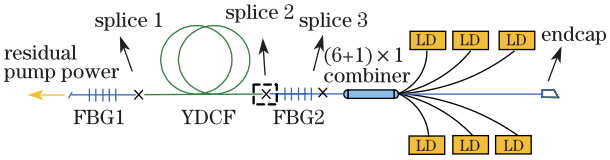

Fig. 5. Experimental arrangement of the backward-pumped, all-fiber laser.

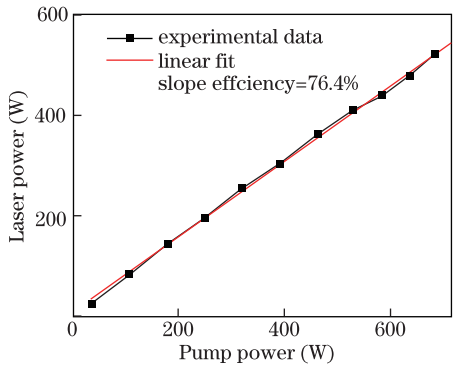

Fig. 6. Laser output power versus pump power.

coupler (FBG2, $R \approx 10\%$ for LP_{01} mode at 1 079 nm). The other end of FBG1 was cleaved at an angle of approximately 6° to avoid back-reflection into the laser oscillator. A 400-μm core-less endcap with a length of 1.5 mm was spliced to FBG2, which was also cleaved at an angle of 6° to minimize back-reflection and prevent surface damage. A total of 6 120-W fiber-pigtailed laser diodes emitting at 976 nm were used as pump sources.

As the pump light launches, the temperature peaks at the splice joint between FBG2 and YDCF (splice2)[8], because the gain fiber has the strongest pump absorption, and backward-pumping makes the stimulated forward laser pass through the joint again. The fiber fusion splice induces a non-guided pump or signal power loss, and causes a rise in temperature. The key splice was held in a temperature-controlled, straight, metallic U-groove with the proper TIM, because highly efficient thermal management was needed for the splice to achieve a lower thermal contact resistance and to prevent possible thermal damage to the fiber coating (Fig. 3(c)). The remaining gain fiber was wrapped in a metallic disc with a 25-cm diameter; this was engraved with U-grooves and

was water-cooled to a constant temperature of 20 °C.

Figure 6 shows the laser output power characteristics. The maximum laser power of the system is 550 W at 1 079.59 nm, and the total coupled pump power is 714 W. The system has an optical-to-optical conversion efficiency of 77%. The slope efficiency is 76.4%, and the linearity is good. The laser output does not exhibit roll-over even at the highest output power, indicating that the system is free from thermal damage.

Figure 7 shows the splice surface temperature versus the total power (of both the backward pumping power and the forward laser power) passing through splice 2. The splice surface temperature increases as the power increases. Due to the good cooling design, when the total power is 1.26 kW, the maximum temperature reaches only 47 °C, which is below the long-term reliability requirement of 80 °C. Given that the equivalent surface temperature increase is only 0.019 K/W, it can pass with over 3-kW power within the acceptable long-term temperature limit.

Figure 8 shows the laser spectrum of the system. The emission is centered at 1 079.6 nm, and the full-width at half-maximum (FWHM) of the laser spectrum is approximately 0.9 nm. No nonlinear signatures are also observed. The beam quality factor M^2 was measured using a PRIMES laser quality monitor. Without any mode-selecting technology, the M^2 factor has a value of 1.35.

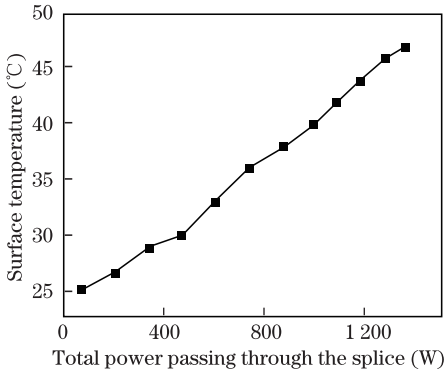

Fig. 7. Splice surface temperature versus the total power passing through splice 2.

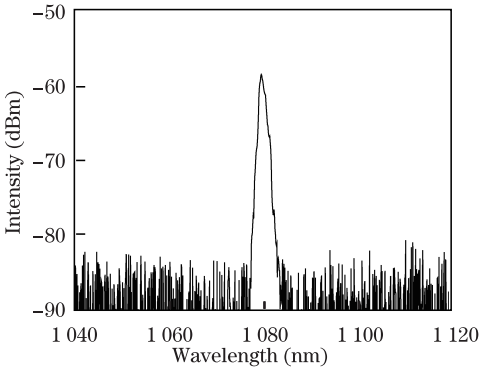

Fig. 8. Laser spectrum of the fiber laser.

In conclusion, we demonstrate an effective fiber cooling method. The thermal properties of three different cooling equipment are discussed and verified experimentally based on thermal contact resistances. The appropriate cooling apparatus is then used on the active fibers and fiber-to-fiber splices of a continuous wave (CW) all-fiber laser system. An output power of 550 W is achieved under a coupled pump power of 714 W, which yields an optical-to-optical conversion efficiency of approximately 77% and a slope efficiency of 76.4%. When a total power of 1.26 kW (from backward pumping and forward laser) passes through the splice joint, into which the pump light launches, the surface temperature is only 47 °C. Therefore, the surface temperature increase is only 0.019 K/W and can sustain 3 kW of total passing power.

This work was supported by the National Science and Technology Major Project (No. 2010ZX04013), the National "863" Program of China (No. 2011AA030201), the Shanghai Rising-Star Program (No. 09QB1401700), the Natural Science Foundation of Shanghai (No. 102R1433600), and the National Natural Science Foundation of China (No. 60908011).

References

1. B. Zhao, K. Duan, W. Zhao, C. Li, and Y. Wang, Chin. Opt. Lett. **8,** 404 (2010).
2. X. Dong, H. Xiao, S. Xu, Z. Pan, Y. Ma, X. Wang, P. Zhou, and Z. Yang, Chin. Opt. Lett. **9,** 111404 (2011).
3. C. Wirth, O. Schmidt, I. Tsybin, T. Schreiber, T. Peschel, F. Brückner, T. Clausnitzer, J. Limpert, R. Eberhardt, A. Tünnermann, M. Gowin, E. ten Have, K. Ludewigt, and M. Jung, Opt. Express **17,** 1178 (2009).
4. D. C. Brown and H. J. Hoffman, IEEE J. Sel. Top. Quantum Electron. **37,** 207 (2001).
5. Y. Wang, C. Q. Xu, and H. Po, IEEE Photon. Technol. Lett. **16**, 63 (2004).
6. N. A. Brilliant and K. Lagonik, Opt. Lett. **26,** 1669 (2001).
7. M.-A. Lapointe, S. Chatigny, M. Piché, M. Cain-Skaff, and J.-N. Maran, Proc. SPIE **7195,** 719511 (2009).
8. Y. Fan, B. He, J. Zhou, J. Zheng, H. Liu, Y. Wei, Y. Dong, and Q. Lou, Opt. Express **19,** 15162 (2011).
9. B. Zintzen, T. Langer, J. Geiger, D. Hoffmann, and P. Loosen, Opt. Express **15,** 16787 (2007).
10. J. P. Gwinn and R. L. Webb, Microelectron. J. **34,** 215 (2003).
11. J. W. Kim, D. Y. Shen, Jayanta K. Sahu, and W. Andrew Clarkson, IEEE J. Sel. Top. Quantum Electron. **15,** 361 (2009).
12. P. Yan, A. Xu, and M. Gong, Opt. Eng. **45,** 124201 (2006).